A COMPACT AND RUGGED HYPERSPECTRAL CAMERA FOR REMOTE SENSING BASED ON A BIREFRINGENT ULTRASTABLE COMMON-PATH INTERFEROMETER

Antonio Perri[1], Fabrizio Preda[1], Dario Polli[1,2,3], Giulio Cerullo[1,2,3], Cristian Manzoni[3]

[1] *NIREOS S.R.L., Via G. Durando 39, 20158 Milano (Italy)* www.nireos.com

[2]*Dipartimento di Fisica, Politecnico di Milano, Piazza L. da Vinci 32, I-20133 Milano, Italy*

[3] *IFN-CNR Piazza Leonardo da Vinci 32, I-20133 Milano, Italy*

ABSTRACT

Spectral imaging is a method to acquire the spectrum of the light for each point in the image of a scene. A powerful method to acquire hyperspectral images is to combine classical imaging with Fourier-transform spectrometry. This technique is based on interferometry, and is hence technically challenging as it requires to generate field replicas with delay controlled within a small fraction (1/100 or better) of the optical cycle. Standard FT spectrometers are heavy, cumbersome and too sensitive to mechanical and thermal perturbations for use in portable devices or for deployment in space applications.

Here we propose and experimentally validate a compact FT-based hyperspectral camera, in which the FT module is the innovative ultra-stable birefringent common-path interferometer (the Translating-Wedge-Based Identical Pulses eNcoding System, TWINS). TWINS has intrinsic interferometric stability, it has light weight and is ultracompact, which make our FT-based hyperspectral camera an ideal device for portable, on-field and spaceborne applications.

Our prototype camera is able to measure absolute reflectance and fluorescence with very high spectral accuracy in the visible and near-infrared spectral range and can be extended to the spectroscopically rich thermal infrared range (3-10 μm) using suitable birefringent materials and detectors. We will also present some examples of application.

1. INTRODUCTION

Many applications in remote sensing require measurement of the light spectrum in the mid-infrared (MIR) range, from 3 to 14 μm, which is resonant with vibrational transitions of molecules. Examples are monitoring of the plastic waste in the ocean, tracking of oil spills, identification of fire hazards or detection of atmospheric gases.

There are two main methods to measure a light spectrum: the frequency-domain and the time-domain approach. In the frequency-domain technique, a prism or grating disperses the light frequency components, which are individually measured by the elements of a multichannel detector. In the time-domain approach, the light is split by an interferometer in two delayed and collinear replicas, whose interference pattern is measured by one detector as a function of their delay. This produces an interferogram, whose Fourier-Transform (FT) yields the intensity spectrum of light. With respect to dispersive spectrometers, the FT method has prominent advantages: (i) higher signal-to-noise ratio in a readout-noise-dominated regime (the Fellgett multiplex advantage); (ii) higher throughput, due to the absence of slits; (iii) flexible spectral resolution, which can be adjusted by varying the total scan delay; (iv) operation with a single detector. Dispersive spectrometers are mostly used in the range from the UV to the near infrared spectral ranges, mainly thanks to the low-cost silicon detector arrays; on the other hand, FT spectroscopy finds its main field of application in the MIR spectral range, in which light detections requires HgCdTe (Mercury Cadmium Telluride, MCT); not only these detectors are way more expensive than silicon ones, but they also have high read-out noise even at cryogenic temperatures. For this reason, spectrometers in the MIR are almost exclusively based on the FT approach.

In the FT approach, the splitting is typically performed by an amplitude division interferometer, such as the Michelson interferometer shown in Fig. 1(c), in which the input light is divided by a beam

splitter in two replicas which follow different pathways and then recombine. For spaceborne applications, the technical challenges of FT spectrometers based on amplitude division interferometers are: (i) the requirement to control the delay of the replicas within a small fraction (1/100 or better) of the optical cycle, avoiding path-length fluctuations of the separate arms caused by external vibrations; (ii) the requirement to keep the two replicas collinear, avoiding mirror misalignments which can easily occur in the presence of strong accelerations. Standard FTIR spectrometers are heavy, cumbersome and too sensitive for portable devices or for deployment in space applications.

2. A NOVEL COMPACT and ULTRASTABLE BIREFRINGENT INTERFEROMETER

Recently, the authors have introduced and patented an FT technology which employs an innovative polarization division interferometer, the Translating-Wedge-Based Identical Pulses eNcoding System (TWINS), which is based on the property that in a birefringent material ordinary and extraordinary light propagate with different velocities [1,2]. The scheme of TWINS is shown in Fig. 1(a): it consists of a birefringent plate followed by two birefringent wedges with adjustable thickness.
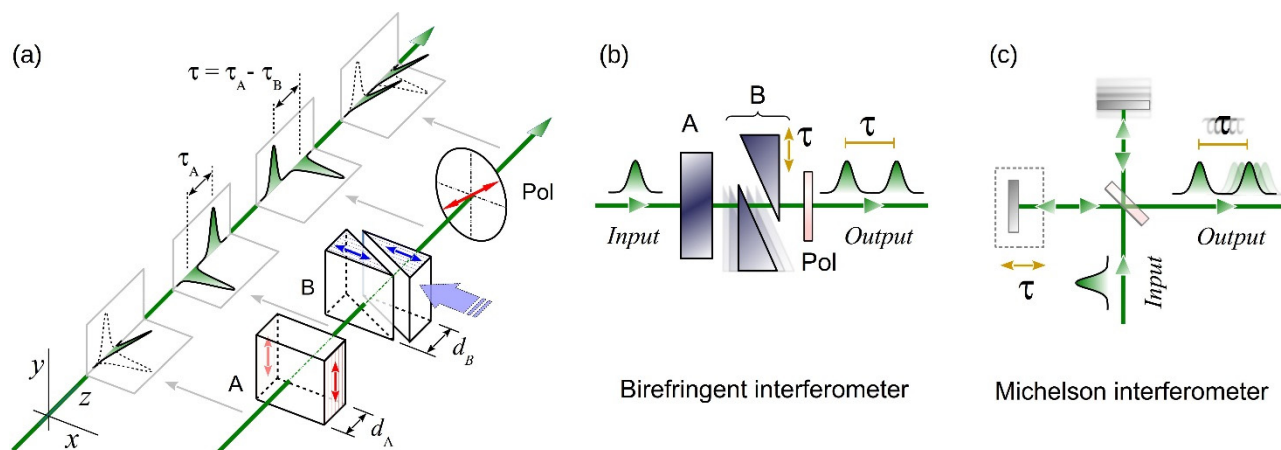

Figure 1: Scheme of the interferometer fir FT spectroscopy. (a) Birefringent interferometer: The input waveform (see left cartoon) is polarized at 45° with respect to the *x* and *y* axes. The birefringent block A (right cartoon) delays the two polarizations by a positive delay τ_A, while block B introduces a variable negative delay τ_B. After the two blocks and the polarizer (pol.), the overall delay of the orthogonally polarized replicas is $\tau_A - \tau_B$. (b, c) Effects of random fluctuations in (b) the birefringent and (c) the traditional (Michelson) interferometers.

The optical axes of the plate and the wedges are orthogonal, so that TWINS generates two field replicas whose relative delay can be precisely controlled by fine tuning of the insertion of one of the wedges, mounted on a translation stage. TWINS has the following unique properties: (i) since both field replicas follow the same optical path, their delay is locked with very high stability and reproducibility and completely insensitive to possible mechanical fluctuations (see Fig. 1(b,c)); (ii) the device demultiplies any transverse translation of the wedges, allowing extremely high delay accuracy; (iii) the device is inherently phase stable and does not require any feedback stabilization as in a standard Michelson interferometer; (iv) the two replicas remain inherently aligned even in the presence of considerable mechanical perturbations of the device. These characteristics make TWINS an ideal device for portable, on field and spaceborne applications, as its footprint and weight are at least one order of magnitude smaller than standard FTIR spectrometer. The authors applied the TWINS technology to variety of devices (FT spectrometers [2], fluorimeters [3], circular dichroism spectrometers [4], hyperspectral cameras [5]…) and has recently spun off a company, NIREOS (www.nireos.com) to commercialize this technology and tighten commercial collaborations with strategic partners.

The spectral coverage of the TWINS interferometer depends on the transparency range of the birefringent plates and wedges; in the visible spectral range, the most performing crystal is α-BBO, a negative uniaxial crystal with transparency from 200 nm to 3.5 micrometers.

The working range can be further extended to the MIR range by using calomel (Hg_2Cl_2) as birefringent material, which combines a very large birefringence ($\Delta n \approx 0.55$) with a broad transparency range (from 400 nm to 20 μm). The calomel TWINS preserves in the MIR the advantages (compactness, long-term stability, delay reproducibility and robustness) of its versions in the visible [6]. For these reasons, a calomel-based TWINS has great potential for a new generation of spaceborne FT instruments with unprecedented compactness, robustness and long-term stability.

3. HYPERSPECTRAL IMAGING with the TWINS BIREFRINGENT INTERFEROMETER

The FT approach for spectroscopy offers a unique advantage also for imaging. An imaging system is made of imaging optics and a 2D detector; by placing the interferometer in the imaging system, it is possible to record in parallel the spectra of all pixels of the two-dimensional scene, a technique also known as hyperspectral imaging (HSI). By using the TWINS birefringent interferometer in an imaging system, we combine the advantages of FT spectroscopy and imaging with the robustness, accuracy and high contrast of TWINS. TWINS applied to FT imaging enables HSI with short acquisition times and high spectral accuracy. A schematic of a TWINS-based hyperspectral camera is shown in Fig. 2.
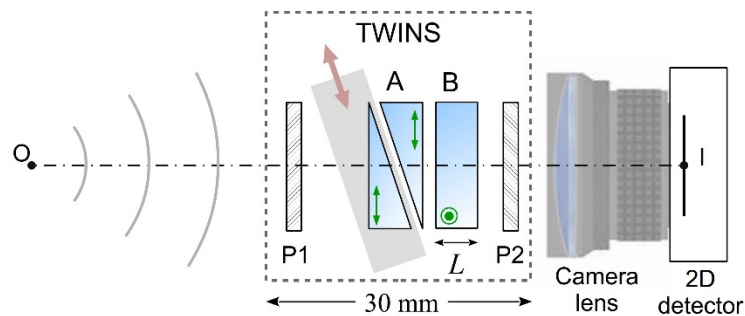

Figure. 2: schematic setup of the hyperspectral camera. P1 and P2: polarizers; A, B: birefringent elements; green double arrow and green circle: optical axes. O: object; I: image.

It consists of three main building blocks: the compact birefringent interferometer, the imaging optics and the monochrome 2D detector. This compact HSI camera can be designed to operate in spectral regions ranging from the visible to the infrared.

3.1 Performances of the TWINS-based HSI in the Visible Spectral Range

The hyperspectral camera was applied for the imaging of objects and works of art, and for remote sensing in the visible spectral range. The 2D detector was a silicon monochrome CMOS camera, which allowed broadband detection in the visible and near infrared spectral range (400-1000 nm).
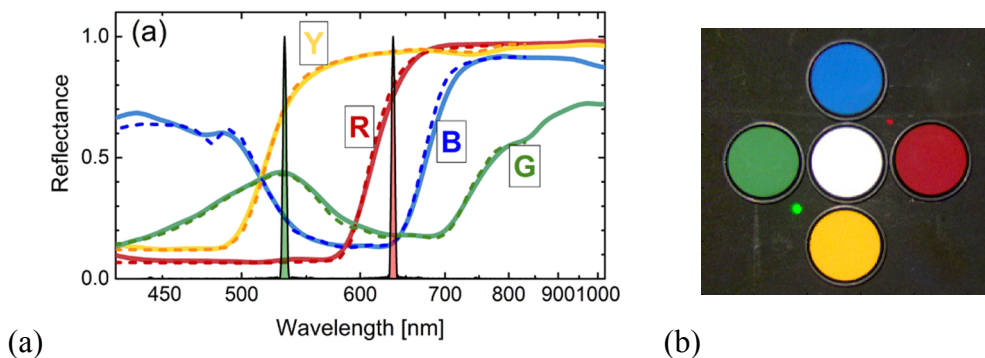

(a)   (b)

Figure 3: test image of calibrated color standards. (a) Absolute spectral reflectance; solid line: measured by HSI camera; dashed line: tabulated reflectance. (b) Reconstruced RGB image.

Figure 3 shows the measurement of a test scene, which consists of 4 colored Spectralon materials (green, blue, red, yellow, G, B, R, Y), acting as calibrated diffusive reflectance standards, and a white Spectralon, with constant reflectance. Panel (a) shows the absolute reflectance spectra of each colored spectralon; the reflectance measured with our HSI (solid lines) perfectly matches the tabulated spectra (dashed lines); the spectral information enables the synthesis of the RGB color image shown in Fig. 3(b). Figure 4 shows the results from remote sensing of a natural landscape, under solar illumination.
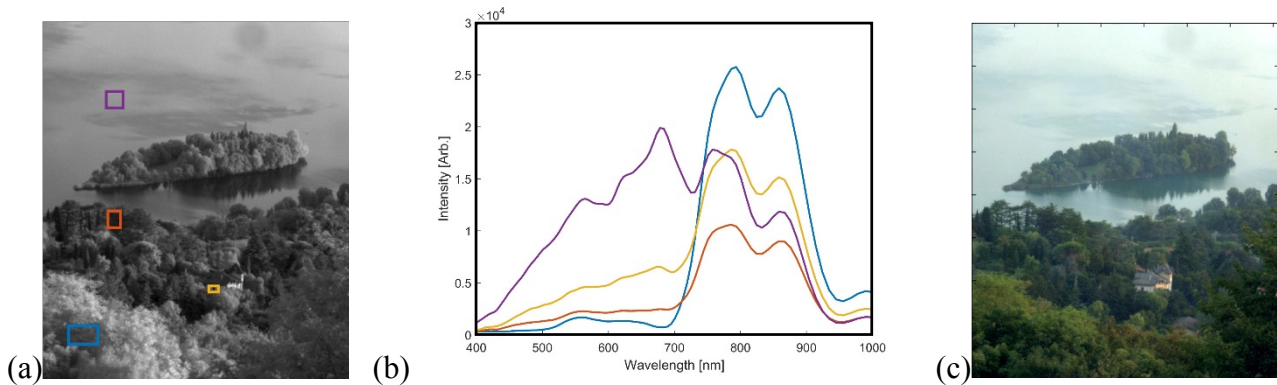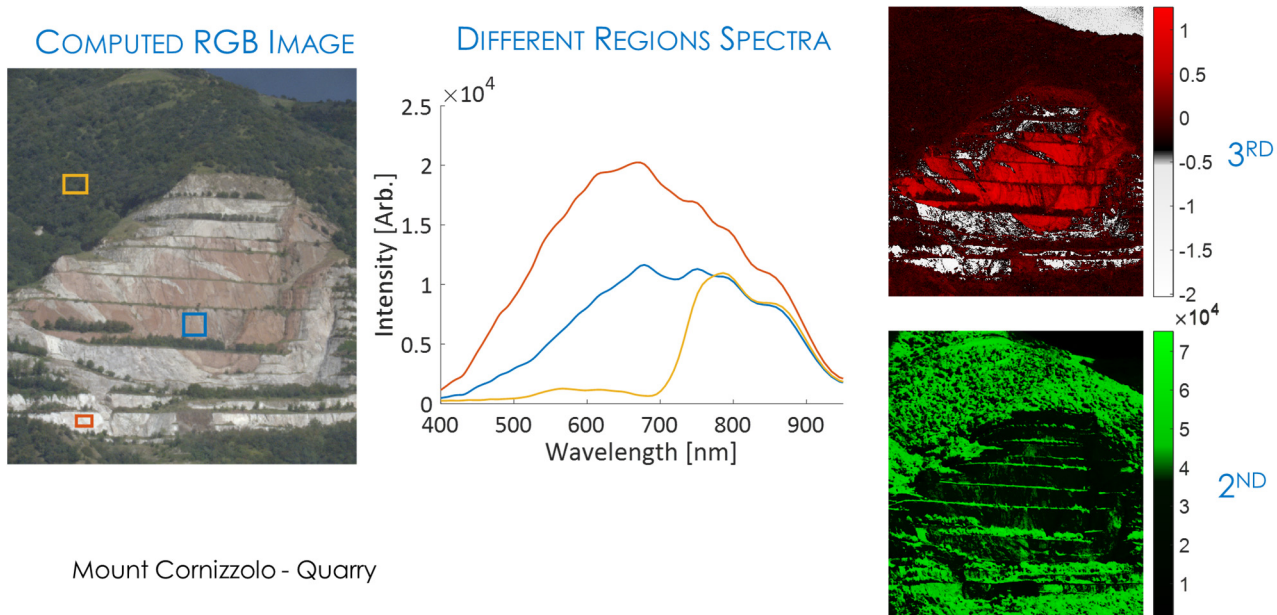

(a)   (b)   (c)

Figure 4: remote HSI of a natural landscape. (a) raw image from the 2D detector; (b) Intensity spectra at selected areas of the image; (c) Reconstruced RGB image.

The spectra at selected points (Fig. 4(b)) clearly show the two fluorescence peaks of chlorophyll and the broad reflectivity of the lake. Panel (c) is the RGB image reconstructed from the spectral information.

Figure 5: remote HSI of a quarry. (a) Reconstrucetd RGB image; (b) Intensity spectra at selected points; (c) preliminary spectral classification, by Principal Components Analysis.

The spectral information, after suitable analysis, also enables remote material identification, as shown in Fig. 5.

4. PERSPECTIVE APPLICATION in the MIR SPECTRAL RANGE

Remote spectral sensing is particularly valuable for satellite or airborne monitoring of Earth. The spectral range carrying the richest information is the **infrared region**, in particular **from 750nm to 14μm**, where two kinds of physico-chemical information can be measured:

(1) the __absorption__ spectrum: it arises from low **molecular/electronic transitions** (at wavelengths shorter than 1 micrometer) and from **vibrational energy levels** associated with chemical bonds of molecules (at wavelengths longer than 1 micrometer). Measuring the infrared absorption spectrum enables the unambiguous identification of molecules and chemical compounds *at the surface* of an object or *in the spa*ce between the object and the detector.

(2) the __surface temperature__ of an object, through the spectral peak of its thermal emission. The wavelength peak of the thermal emission of a black body ranges from from 3 μm for a body at 1000K to 14.5 μm at 200K.

Spectral imaging measures the outward flow of radiation from *the Earth surface* and its *atmosphere* into space. The radiation transmitted by the Earth atmosphere, together with its flux direction, is summarized in Figure 6.
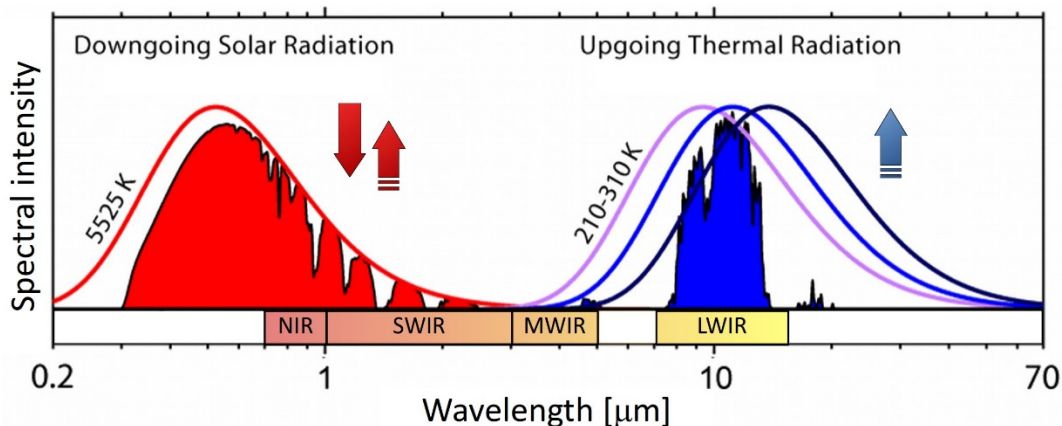

Figure 6: Radiation transmitted by the Earth atmosphere

- The visible and near-infrared light from 300 nm to 3 micrometers (red area) is dominated by an *exogenous* source, the solar radiation; the fraction of solar light which is scattered back to space holds spectral information about the **absorption**, **reflection** and **scattering** properties of molecules and particles of the *land*, *water* and *atmosphere* environments;
- The infrared range between 3 and 15 microns, on the other hand, is *endogenous* since it is mainly the thermal radiation originating from the Earth surface and atmosphere (blue area). The thermal infrared radiation emitted from a volume or surface is substantially different from transmitted or reflected light. From the spectrum of the thermal radiation it is also possible to measure **temperature**, **albedo**, **radiance** and **emissivity** of an object, which enables identifying the composition and temperature of the surface. In addition, the emitted infrared radiation, though similar to blackbody radiation, is banded by the absorption lines from characteristic **vibrational modes**, enabling further fingerprinting of chemical compounds on the surface and in the atmosphere.

The infrared radiation is typically arranged into various sub-bands; following a division scheme based on sensor sensitivity, these sub-bands are (see Fig. 6):

- **Near-infrared (NIR)**: 0.75-1 μm, from the approximate end of the response of the human eye to that of *silicon.*
- **Short-wave infrared (SWIR)**: 1-3 μm, from the cut-off of silicon to that of the edge of the atmospheric window at 3 μm. Extended *InGaAs* covers to about 2.5 μm; the less sensitive *lead salts* also cover this region.
- **Mid-wave infrared (MWIR)**: 3-5 μm, defined by the atmospheric window and covered by *indium antimonide [InSb]*, *mercury cadmium telluride [HgCdTe]* and partially by *lead selenide [PbSe]*.
- **Long-wave infrared (LWIR)**: 7-14 μm, the atmospheric window covered by *HgCdTe* and *microbolometers*.

Since it is associated to thermal emission, the range between 3 and 14 μm is also called **Thermal Infrared (TIR)**. Note that very little TIR light is transmitted in the **5-7 μm** range and beyond 14 μm. As shown in Figure 7, these regions are characterized by **low transmittance** of the atmosphere, mainly due to absorption by water vapor.
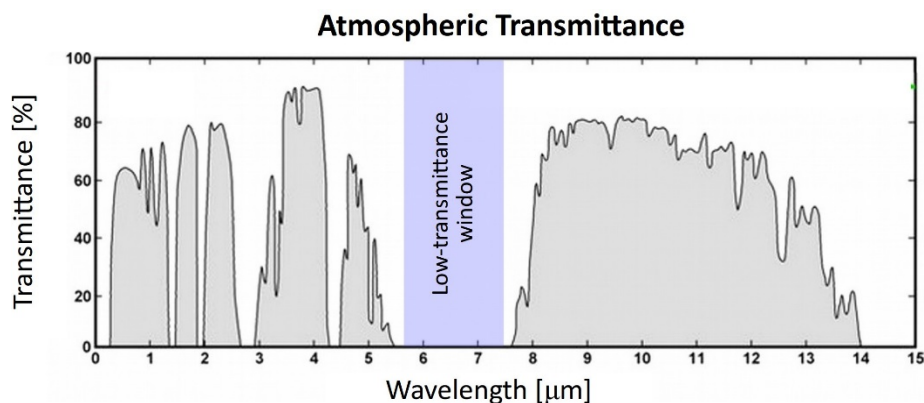

Figure 7: Atmospheric transmittance spectrum

The surface **radiance**, **temperature** and **emissivity** are primarily used for monitoring changes in Earth's surface, such as those related to volcanoes, fires, water, snow and ice distribution, presence and motion of atmospheric gases, greenhouse effect and climatology [7, 8], urbanization, surface energy balance, land use and cover [9].

In particular, spectral imaging in the TIR range enables the detection of

- SILICATE MINERALS. Silicate are the largest and most important class of minerals and make up approximately 90 percent of the Earth's crust. Their relation to the presence of valuable minerals, such as gold and diamonds, is well understood. The reflectance and emissivity spectra of silicate minerals provide a means for their remote discrimination and identification from airborne images [10]. Silicate are also present in the dust, and enable monitoring the Earth's mineral dust cycle. The cycle impacts on the warming or cooling of the atmosphere, and hence on climate.

- WILDFIRES: Emissions from biomass burning are widely recognized as a significant source of pollution affecting atmospheric chemistry, photochemistry, and trace gas concentrations. Hence measurements of active fires in the TIR measurements can be used to calculate carbon emissions [11].

- VOLCANOES: Volcanic eruptions inject large quantities of ash into the atmosphere and ash clouds pose a hazard to aviation. The location of these ash clouds, the amount of ash they

contain, and how these parameters change over time, needs to be quantified in a timely manner if the economic costs, and the danger posed to air passengers, are to be minimized. Together with ashes, volcanoes also release sulfur dioxide (SO_2) gas. Measuring its concentration is crucial for determining the degassing budget of volcanoes but also to estimate the amount of volcanic gases driving explosions [12]. Figure 8 shows multispectral TIR images of the Augustine volcano (Kenai Peninsula Borough of southcentral coastal Alaska), measured from ASTER (Advanced Spaceborne Thermal Emission and Reflection Radiometer), a high resolution imaging instrument that is flying on the Terra satellite.
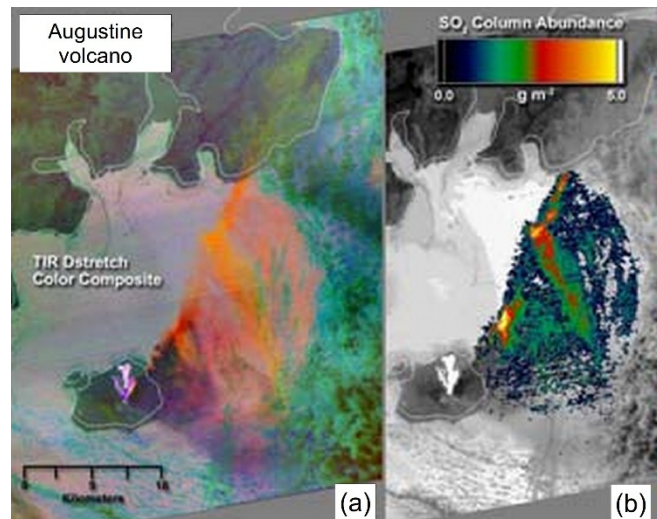

Figure 8: (a) night-time multispectral TIR image of Augustine Volcano showing hot pyroclastic flow deposits (bright in TIR) and eruption plume. Colors indicate spectral variations between materials entrained in plume. Magenta: mixtures of water droplets (steam) and silicate ash; red, yellow, and orange: mixtures of ash and SO_2. (b) SO_2 map derived from ASTER TIR data.

- **WATER USE AND AVAILABILITY:** knowing natural and anthropogenic land-cover together with **soil moisture** is important to local and regional water management. A valuable metric for estimating evapotranspiration and available water is the land surface temperature. In addition, **snow and ice** albedo plays a significant role in the regional and global energy balance. Snow grainsize and liquid water content can be derived simultaneously from hyperspectral images in the SWIR infrared range.

- **ATMOSPHERIC GASES AND GREENHOUSE EFFECT:** Earth's surface, warmed by the solar radiation to a temperature around 255 K, radiates long-wavelength, infrared heat in the range of 4–100 μm. [13]. At these wavelengths, **greenhouse gases** that were largely transparent to incoming solar radiation are more absorbent, and reradiate in all directions, both upwards and downwards. Increasing the concentration of the gases increases the amount of absorption and re-radiation, and thereby further warms the layers and ultimately the surface below. The major gases contributing to the greenhouse effect are water vapor, carbon dioxide, methane and ozone, and have well-defined absorption lines in the TIR spectral region.

5. CONCLUSIONS

In this paper, we have introduced a novel system for hyperspectral imaging, based on FT spectroscopy. The interferometer is the innovative ultra-stable birefringent common-path interferometer TWINS, which has unique advantages over traditional interferometers, from the intrinsic interferometric stability and reproducibility, to the light weight (few-kg) and ultracompact

(<1 dm^3) volume. These characteristics make our FT-based hyperspectral camera an ideal device for portable, on-field and spaceborne applications.

Our prototype camera is able to measure absolute reflectance and fluorescence with very high spectral accuracy in the visible and near-infrared spectral range and can be extended to the spectroscopically rich thermal infrared range (3-10 μm) using suitable birefringent materials and detectors

References:

1. D. Brida, C. Manzoni, and G. Cerullo, "Phase-locked pulses for two-dimensional spectroscopy by a birefringent delay line," Opt. Lett. **37**, 3027–3029 (2012).
2. A. Oriana, J. Réhault, F. Preda, D. Polli, and G. Cerullo, "Scanning Fourier transform spectrometer in the visible range based on birefringent wedges," J. Opt. Soc. Am. A **33**, 1415–1420 (2016).
3. A. Perri, F. Preda, C. D'Andrea, E. Thyrhaug, G. Cerullo, D. Polli, and J. Hauer, "Excitation-emission Fourier-transform spectroscopy based on a birefringent interferometer," Opt. Express **25**, A483-A490 (2017).
4. F Preda, A. Perri, J. Réhault, B. Dutta, J. Helbing, G. Cerullo, and D. Polli, "Time-domain measurement of optical activity by an ultrastable common-path interferometer," Opt. Lett. **43**, 1882-1885 (2018).
5. A. Perri, B. E. Nogueira de Faria, D. C. T. Ferreira, D. Polli, D. Comelli, G. Valentini, G. Cerullo, and C. Manzoni, "A Hyperspectral Camera for Remote Sensing based on a Birefringent Ultrastable Common-Path Interferometer," in Light, Energy and the Environment 2018 (E2, FTS, HISE, SOLAR, SSL), OSA Technical Digest (Optical Society of America, 2018), paper HM3C.4.
6. J. Réhault, R. Borrego-Varillas, A. Oriana, C. Manzoni, C. P. Hauri, J. Helbing, and G. Cerullo, "Fourier transform spectroscopy in the vibrational fingerprint region with a birefringent interferometer," Opt. Express **25**, 4403-4413 (2017).
7. M. C. Anderson, J.M. Norman, J.R. Mecikalski, J.A. Otkin, & W.P. Kustas, "A climatological study of evapotranspiration and moisture stress across the continental United States based on thermal remote sensing: 2. Surface moisture climatology". Journal of Geophysical ResearchAtmospheres 112, D11 (2007)
8. M.L. Jin, & R.E. Dickinson, "Land surface skin temperature climatology: benefitting from the strengths of satellite observations". Environmental Research Letters 5, 4 (2010).
9. A.N. French, T.J. Schmugge, J.C. Ritchie, A. Hsu, F. Jacob, & K. Ogawa, "Detecting land cover change at the Jornada Experimental Range, New Mexico with ASTER emissivities". Remote Sensing of Environment 112, 1730-1748 (2008)
10. S.J. Hook, J.E. Dmochowski, K.A. Howard, L.C. Rowan, K.E. Karlstrom, & J.M. Stock, "Mapping variations in weight percent silica measured from multispectral thermal infrared imagery - Examples from the Hiller Mountains, Nevada, USA and Tres Virgenes-La Reforma, Baja California Sur, Mexico", Remote Sensing of Environment 95, 273-289 (2005).
11. Y. J. Kaufman, C. O. Justice, L. P. Flynn, J. D. Kendall, E. M. Prins, L. Giglio, D. E. Ward, W. P. Menzel, and A. W. Setzer, "Potential global fire monitoring from EOS-MODIS". Journal of Geophysical Research 103, 32215–32238 (1998). .
12. G. Tamburello et al., "Passive vs. active degassing modes at an open-vent volcano (Stromboli, Italy)," Earth and Planetary Science Letters, 359-360, 106-116 (2012).
13. John F. B. Mitchell, "The "Greenhouse" effect and Climate Change". Reviews of Geophysics 27, 115–139 (1989).